Excited State Dynamics in Chlorophyll-Based Antennae: The Role of Transfer Equilibrium

Philip D. Laible, Warren Zipfel, and Thomas G. Owens
Section of Plant Biology, Cornell University, Ithaca, New York 14853-5908

ABSTRACT We present computer simulations of excited state dynamics in models of PS I and PS II which are based upon known structural and spectral properties of the antennae. In particular, these models constrain the pigment binding sites to three-dimensional volumes determined from molecular properties of the antenna complexes. The simulations demonstrate that within a 10–30 ps after light absorption, rapid energy transfer among coupled antenna chlorophylls leads to a quasiequilibrium state in which the fraction of the excited state on any antenna chlorophyll, normalized to the total excited state remaining on the model, remains constant with time. We describe this quasiequilibrium state as a "transfer equilibrium" (TE) state because of its dependence on the rates of processes that couple excited state motion and quenching in the antenna as well as on the individual antenna site energies and temperature. The TE state is not a true equilibrium in that loss of the excited state primarily due to photochemistry (but also due to fluorescence, thermal emission, and intersystem crossing) continues once TE is established. Depending on the dynamics of the system, the normalized distribution of excited state at TE may differ substantially from the Boltzmann distribution (the state of the model at infinite time in the absence of any avenues for decay of excited state). The models predict lifetimes, equilibration times, and photochemical yields that are in agreement with experimental data and affirm trap-limited dynamics in both photosystems. The rapid occurrence of TE states implies that any excited state dynamics that depends on antenna structure and excitation wavelength must occur before the TE state is established. We demonstrate that the excited state distribution of the TE state is central to determining the excited state lifetime and quantum efficiency of photochemistry.

INTRODUCTION

The primary functions of light-harvesting complexes in the early events in photosynthesis are the absorption of light and efficient transfer of excited state energy to the reaction center where primary charge separation occurs. During the time the excited state resides in the antenna, the processes of fluorescence, thermal emission, and intersystem crossing compete for the excited state and ultimately limit the photochemical efficiency of the system. However, it is in part due to the presence of these measurable competing processes that information on the structure and function of the antennae may be obtained. Time-resolved fluorescence studies are one way excited state motion and trapping can be probed through the measurement of excited state decay components (exponentially decaying lifetimes and associated amplitudes) and their dependence upon excitation and emission wavelengths (Holzwarth, 1989; 1991).

Many time-resolved fluorescence studies on various photosynthetic systems reveal complex decay-associated spectra. Based upon the shape of the spectra and the relative magnitude of the lifetimes, the decays are assigned to processes within the functional antenna/reaction center complex. Several processes are known to contribute to the observation of multiexponential decays. Among these processes are bulk transfer from short to long wavelength-absorbing pigments leading to spectral redistribution of excited state (Turconi et al., 1993; Zipfel, 1993), electron transport (Schatz et al., 1988; Zipfel, 1993), antenna size heterogeneity or state transitions (Roelofs et al., 1992; Bruce et al. 1985; 1986), and transfer between spatially and/or spectrally segregated pigment pools within chl-based (Knox and Lin, 1988; Lin and Knox, 1988; 1991; Wittmershaus et al., 1985; Turconi et al., 1993) and phycobilisome-based (Biggins and Bruce, 1988; Suter and Holzwarth, 1987; Holzwarth et al., 1987; Mullineaux and Holzwarth, 1991) antennae at both room and low temperature. Although an understanding of the origin and nature of multiexponential decays is essential for the complete understanding of excited state motion and trapping, this report focuses primarily on the photochemically limited lifetimes of excited states which dominate decays in photosynthetic systems with high photochemical efficiencies.

At the present time, there are substantial experimental limitations (primarily time resolution and spectral overlap) which preclude the determination of detailed structural features of photosynthetic antennae from experimentally determined excited state lifetimes and amplitudes (Wittmershaus et al., 1985; Lin and Knox, 1988; 1991; Biggins and Bruce, 1988; Suter and Holzwarth, 1987; Mullineaux and Holzwarth, 1991; Jean et al., 1989). Computer simulations of excited state dynamics in models of photosynthetic antennae may be complementary to experimental studies, providing information that is critical to the interpretation of experimental data, as well as a detailed knowledge of how antenna structure can dictate excited state motion and trapping. The time-dependent motion and decay of the excited state in photosynthetic systems has been simulated using random walk

Received for publication 7 June 1993 and in final form 6 December 1993.
Address reprint requests to Thomas G. Owens at the Section of Plant Biology, Cornell University, Ithaca, NY 14853-5908. Tel.: 607-255-8516; Fax: 607-255-5407; e-mail: tgo2@cornell.edu.

0006-3495/94/03/844/17 $2.00

theory (Montroll, 1969), transition probability matrix methods (Seely, 1973; Fetisova et al., 1985), and analytical (Knox, 1968; Pearlstein, 1982; 1984; 1992) or numerical (Shipman, 1980; Jean et al., 1989; Beauregard et al., 1991; Zipfel, 1993) solutions to the Pauli master equation.

In many studies, models of reaction center/core antenna complexes were severely constrained in order to insure a systematic (analytical) solution to the Pauli master equation. For example, the requirement for equal Förster rate constants between all nearest-neighbor sites restricts models to those with isoenergetic antenna pigments placed at lattice sites within a regular array with an internally located reaction center (Pearlstein, 1982). Nonetheless, these simulation techniques have provided valuable information on excited state dynamics in a variety of photosynthetic antenna systems. As techniques matured, allowing one to obtain numerical solutions to more complex models of photosynthetic systems, the two-dimensional (2D) nature of the initial models persisted (Jean et al., 1989; Beauregard et al., 1991). Zipfel (1993) has demonstrated that the use of 2D models places significant limitations on the interpretation of excited state dynamics when comparing computer simulations with experimental results.

In the present study, we introduce models for studying excited state dynamics of PS I and PS II in which the pigment binding sites are constrained to volumes (three-dimensional) determined from known properties of the antenna complexes. The simulation technique that we have chosen is to obtain an exact numerical solution to the Pauli master equation; this procedure places no structural or functional limitations on the model. The phenomenon which we explore is not new but is similar to the zero-mode dominance of analytical solutions proposed by Pearlstein (1982; 1984; 1991), Knox (1968; 1986), and Borisov (1990) and that briefly suggested in the discussion of Robinson (1967), Ross and Calvin (1967), and Zankel and Clayton (1969). Several new terms are defined in the discussion of this phenomenon and are summarized in Appendix A.

SIMULATION METHODS

The procedure that we have adopted for computer simulation of excited state migration and trapping dynamics in model photosynthetic systems is essentially that described in Jean et al. (1989) with some important modifications. Our objective is to use as much structural information and appropriate physical laws to describe the system. Where information is lacking, assumptions are made (justified by our current state-of-knowledge) while still applying the most appropriate physical laws.

Initially, a physical model is constructed by assigning positions, orientations, and site energies (absorption maxima) to each of the N pigment binding sites in the model. Pairwise transfer of energy between all sites is assumed to occur via an incoherent hopping mechanism described by Förster (1965). This assumption is not required by the simulation protocol as monopole or higher order Coulombic interactions could be included (Chang, 1977) as could exchange interactions for closer pigment pairs. Even in the event of strong coupling between sites, Knox and Gülen (1993) suggested that Förster is still an appropriate description of the coupling. Orientation factors are explicitly calculated. With the exception of the reaction center (see below), all of the orientations are randomly assigned giving a range of orientation factors between 0 and 4.

A value of 1.0 is chosen for the index of refraction (η) for nearest-neighbor pairs in the Förster transfer equation; values of η between 1.2 and 1.4 were randomly assigned for all other pairs. As discussed in Moog et al. (1984), the value of η reflects the properties of the medium (amino acids, other pigments, ions, water molecules, etc.) found between the donor and acceptor molecules which are *not* already taken into account by absorption of the pigments. Since neighboring pigments are bound in close proximity (mean spacing of 10–15 Å), absorption already takes into account index of refraction in the immediate vicinity of nearest-neighbor pigments (Moog et al., 1984).

In all models the reaction center is assumed to be dimeric with double the oscillator strength of the antenna pigments. For simplicity, a single unimolecular rate constant ($k_f = (1\ \text{ns})^{-1}$) for decay of excited states on each pigment site is assigned representing the sum of the rate constants for fluorescence, thermal emission, and intersystem crossing. However, the simulation protocol allows for unique assignment of rate constants for all sites. The photochemical rate constant, k_p, on the reaction center is assigned a value of $(2.8\ \text{ps})^{-1}$. Photochemistry is modeled as an irreversible process. Thus, our simulations are designed to examine excited state dynamics without the coupling of reversible electron transport steps. Such coupling may result in additional contributions to the fluorescence decay kinetics (Schatz et al., 1988; Zipfel, 1993). However, Zipfel (1993) also showed with simulations using similar models that neglecting the contributions of electron transport does not alter the fundamental conclusions of this paper.

The Pauli master equation describing this system of N coupled first-order differential equations (where N also refers to the number of pigment-binding sites in the model) is given by

$$d\mathbf{p}(t)/dt = \mathbf{W} \cdot \mathbf{p}(t) \tag{1}$$

where $\mathbf{p}(t)$ is a vector of site occupation probabilities, and $\mathbf{W}$ is an $N \times N$ rate matrix of pairwise transfer and unimolecular decay rates. The general solution to the Pauli master equation is conveniently expressed as N time-dependent site occupation probabilities, where the time-dependent site occupation probability for pigment i, $p_i(t)$, is given by

$$p_i(t) = c_1 x_{i1} e^{\lambda_1 t} + c_2 x_{i2} e^{\lambda_2 t} + \cdots + c_N x_{iN} e^{\lambda_N t} \tag{2}$$

Here, the λ_j terms refer to the eigenvalues of the rate matrix[1], the

[1] In our models in which losses of excited state are irreversible, all of the eigenvalues of the rate matrix must be negative. We have ordered the eigenvalues according to $|\lambda_j|$ such that $|\lambda_1| < |\lambda_j|$ with $1 < j \leq N$. The subscript j refers to a specific eigenvalue, not pigment.

x_{ij} terms refer to eigenvector elements corresponding to pigment i and eigenvalue j, and the c_j terms refer to constants determined such that $p_i(t)$ terms at $t = 0$ are equal to the initial distribution $p_i(0)$ terms. The initial excited state distribution, $\mathbf{p}(0)$, may be assigned in any arbitrary fashion with the constraints that $\Sigma p_i(0) = 1$ and $p_i(0) \geq 0$ for all i. However, to duplicate experimental conditions, the value of $\mathbf{p}(0)$ is determined by the relative absorption cross-section of each individual pigment at the excitation wavelength. Simulation results presented are averages over 15 random configurations. Averaging over three times as many configurations did not quantitatively change the results as the pigment binding sites in the models are highly constrained (see below). Simulated lifetimes ($\tau_i = -1/\lambda_i$) are nearly identical to experimental lifetimes which would be obtained by fitting single-photon counting data in the absence of noise and in the absence of an instrument response function. In the absence of electron transfer and antenna-size heterogeneity, the largest eigenvalue gives rise to the photochemically limited lifetime τ (where $\tau = -1/\lambda_1$). Photochemical yield ϕ_p is calculated as:

$$\phi_p = \frac{k_p \int_0^\infty p_{rc}(t)\,dt}{k_p \int_0^\infty p_{rc}(t)\,dt + k_f \sum_{i=1}^{N} \int_0^\infty p_i(t)\,dt} \qquad (3)$$

An important modification from the procedure of Jean et al. (1989) is our use of realistic, asymmetric spectral lineshapes for chlorophyll (chl) *a* absorption and emission based upon the in vitro data of Shipman and Housman (1979). Previous simulations (Jean et al., 1989; Beauregard et al., 1991; Jia et al., 1992) assumed simple Gaussian lineshapes for chl *a*, determined the forward transfer rates by numerical integration of Förster overlap integrals, and calculated reverse transfer rates using the Boltzmann factors ($e^{-\Delta E/kt}$; with the energy difference measured as differences in peak energies of the pigments) as a criterion for detailed balance. In the present study, values of the Förster rates for both forward and reverse transfer were determined using analytic expressions for the overlap integral based upon assumed chl *a* lineshapes having constant absorption and emission bandwidths (Shipman and Housman, 1979) and a constant Stokes shift of 150 cm^{-1}. Typically, the range of nearest neighbor transfer rate constants were between 1–30 and 0.01–8 ps^{-1} for forward and reverse transfer, respectively.

In our simulations we used an improved procedure to calculate the eigenvalues, eigenvectors, and inverse of the eigenvector matrix. The details of this procedure are presented in Zipfel (1993). Briefly, the procedure utilizes a similarity transform of the rate matrix to take advantage of the properties of symmetric matrices. The transform is based upon the Boltzmann equilibrium distribution of the excited state; thus, detailed balance is an inherent property of the system. The technique removes potential problems due to the accumulation of floating point errors in calculating the eigensystem of large, real matrices (Zipfel, 1993).

MODELS

PS I core antenna/reaction center complex

Our PS I model consists of the reaction center/core antenna complex which binds P700 and about 120 core chl *a* pigments in a dimeric protein complex made up of the 83-kDa products of the *psaA* and *psaB* genes (Golbeck and Bryant, 1991; Bruce and Malkin, 1988; Bryant et al., 1987; Golbeck, 1987). Based on structural studies of the bacterial reaction center (Deisenhofer and Michel, 1989), LHC II (Kühlbrandt and Wang, 1991), and PS I (Krauss et al., 1993), pigment binding sites are restricted to the α-helices in the membrane-spanning region.

The pigment binding volume of the complex is estimated from the molecular mass of the pigment-binding proteins (166 kDa) and from a specific molecular volume of 3300 $Å^3$/kDa (Kühlbrandt and Wang, 1991). Although this value is larger than that for average proteins (1200–1400 $Å^3$/kDa (Teller, 1976)) or the bacterial RC (1500 $Å^3$/kDa (Deisenhofer and Michel, 1989)), it was selected because the protein/pigment ratio in the PS I core (1.28 kDa/pigment) is more similar to that of LHC II (1.67 kDa/pigment) than the bacterial reaction center (24.0 kDa/pigment). By restricting the pigment binding sites to the membrane-spanning region (40% of the protein mass based upon hydropathy plots (Fish et al., 1985)), we arrive at a binding volume of 219,000 $Å^3$ per complex. Mean pigment spacing in the model is estimated assuming that this binding volume was filled with 120 sites in either face-centered or body-centered lattices. The geometric mean spacing for these two lattice structures is 12.8 Å. This compares with nearest neighbor spacings in the range of 8–15 Å in PS I (Krauss et al., 1993) and 9–14 Å in LHC II (Kühlbrandt and Wang, 1991).

The binding volume of the complex is modeled to be an ellipsoid with its minor axis (40 Å) normal to the membrane plane and a major axis of 104 Å in the membrane plane. These dimensions are nearly identical to the membrane-spanning region of the PS I core complex determined by x-ray crystallography (Krauss et al., 1993). P700 is positioned on one end of the minor axis on the surface of the complex (Krauss et al., 1993). The complex also binds several components involved in vectorial electron transport from P700 to the opposite side of the membrane (Golbeck and Bryant, 1991; Krauss et al., 1993). Due to restrictions imposed by the presence of electron transport components (Pearlstein, 1992), the four nearest neighbors of P700 are placed at adjacent corners of a body-centered cube (with P700 in the central site). The plane defined by the four nearest neighbors is perpendicular to the membrane normal and interior to the binding volume. Two of these nearest neighbors are assigned absorption maxima at 705 nm (Butler, 1961). The presence of antenna spectral forms with S_1 energies below that of P700 are required to account for the steady state emission of PS I (Zipfel, 1993; Turconi et al., 1993) and to model the temperature-dependent decay of excited states in PS I (Werst et al., 1992; Jia et al., 1992). The remaining pigment sites are randomly distributed with a

minimum separation of 12.0 and a mean spacing of 12.8 Å. The chl *a* spectral forms modeled in the complex are those determined by Gaussian deconvolution of the PS I core complex absorption (Owens et al., 1988) with the inclusion of two 705-nm pigments (Table 1). However, models including a larger number of spectral forms (e.g., those described by Trissl et al. (1993)) do not differ quantitatively from those reported here. P700 is modeled as a dimer of chl *a* with an oscillator strength twice that of the antenna chls. The transition dipole of P700 is set parallel to the membrane normal (Rutherford and Sétif, 1990); all other orientations were randomly assigned.

PS II core antenna/reaction center complex with associated LHC II

The core antenna complex of PS II binds about 45 chl *a* pigments in a dimeric protein complex made up of the 45–51 and 40–45-kDa proteins referred to as CP47 and CP43, respectively (Hansson and Wydrzynski, 1990). The reaction center P680 and five additional pigments are bound in the D1-D2-cytochrome b_{559} reaction center complex (Nanba and Satoh, 1987). Because there is no evidence that energy transfer between the core antenna and reaction center complexes is any slower than transfer within the core antenna, the reaction center/core antenna aggregate is modeled with P680 included within the binding volume of the core antenna apoproteins. The pigment binding volume of the core complex is estimated from the molecular mass (≈90 kDa) and from specific molecular volume of 3300 Å^3/kDa. By restricting the pigment binding sites to the membrane-spanning region (≈50% of the protein mass based upon hydropathy plots (Alt et al., 1984)), we arrive at a binding volume of ≈ 120,000 Å^3 per core complex. Mean pigment spacing in the models is estimated assuming that this binding volume was filled with 45 sites in either face-centered or body-centered lattices. The geometric mean spacing for these two lattices structures is 14.5 Å.

The binding volume of the complex is modeled as an ellipsoid with its minor axis (40 Å) normal to the membrane plane and a major axis of 70 Å in the membrane plane. For comparison, Dekker et al. (1988) estimated the dimensions of a PS II reaction center/core complex from *Synechococcus* to be 130 × 75 × 60 Å (note that our model lacks the volume contributed by the reaction center complex). The position of P680 in the core complex and the geometry of its nearest neighbors are identical to that of P700 in the PS I model. The remaining sites are randomly distributed with a minimum separation of 11 and a mean spacing of 14.5 Å. The chl *a* spectral forms modeled in the complex absorb maximally between 676 and 680 nm (Bassi et al., 1990) and are randomly distributed. The transition dipole of P680 is set parallel to the membrane normal (Deisenhofer and Michel, 1989); all other orientations are randomly assigned.

The contribution of the peripheral LHC II antenna to excited state dynamics in PS II is modeled by coupling two LHC II trimers to the reaction center/core antenna (similar to a PS II_β complex). The structure of the LHC II trimer is based on the data of Kühlbrandt and Wang (1991). The pigment binding volume of each trimer is modeled as a cylinder 73 Å in diameter and 40 Å in height. A total of 45 chl *a* + *b* are bound per trimer (chl *a*/*b* = 1.2 (Hansson and Wydrzynski, 1990)) with a mean spacing of 11 Å. Chl *a* and *b* in LHC II absorb maximally at 672 and 652 nm, respectively (Jennings et al., 1990). Within these constraints, the positions, orientations, and spectral types are randomly distributed in the pigment binding volume. The spacing between the boundaries of LHC II and the core complexes is set to 10 Å (unless noted otherwise). Due to the restraints of the pigment binding volume and minimum pigment spacing, pigments typically reside on the boundaries of the ellipsoidal proteins in our models. Thus, the average pigment spacing for energy transfer between complexes is the same as the spacing between the boundaries of the complexes. Energy transfer between the complexes is limited to spectral forms of chl *a*, chl *b* to chl *a* transfers restricted to LHC II. Spectral composition of the PS II model is summarized in Table 2.

BOLTZMANN DISTRIBUTION

Inherent in the way that the rate matrix is constructed is the property of detailed balance. That is, in the absence of decay processes, the excited state distribution must relax to an equilibrium state that is determined only by the distribution of accessible energies (absorption and emission properties) at each pigment-binding site. We refer to this relaxed distribution as the Boltzmann distribution based upon its maximum entropy properties (Heitler, 1954; van Kampen, 1981)

TABLE 1 Spectral composition of 3D, random models of the PS I reaction center/core antenna complex

Spectral form (A_{max} in nm)	Number of pigments
Reaction center (700)	1
Long λ pigments (705)	2
Core Chl *a* (685)	36
Core Chl *a* (677)	45
Core Chl *a* (667)	36

The spectral composition is basically that determined by gaussian deconvolution of the PS I core antenna absorption (Owens et al., 1988) with the inclusion of two 705-nm spectral form pigments.

TABLE 2 Spectral composition of 3D, random models of the PS II reaction center/core antenna complex with associated LHC II peripheral antennae

Spectral form (A_{max} in nm)	Number of pigments
Reaction center (680)	1
Core Chl *a* (676–680)	45
LHC II Chl *a* (672)	48
LHC II Chl *b* (652)	40

The models contain a total of 134 pigment binding sites (46 within the core and 44 within each LHC II peripheral antenna). The absorption maxima of chl *a* within the core is based upon Bassi et al. (1990). The chl *a* and *b* found within LHC II are assigned an absorption based upon Jennings et al. (1990), and the chl *a*:chl *b* ratio in LHC II is chosen to be 1.2 (Hansson and Wydrzynski, 1990).

and its equivalence to the most probable or maximum likelihood description of the system (Atkins, 1990). The Boltzmann distribution for any given model **p**(B) is comprised of N individual pigment distributions, $p_i(B)$. This Boltzmann distribution is identical to the stationary state in stochastic physics (van Kampen, 1981).

Spectral composition is the sole factor contributing to the Boltzmann distribution, **p**(B). In a homogeneous antenna model with an isoenergetic reaction center, all $p_i(B)$ are exactly $1/N$ (including $p_{rc}(B)$, the Boltzmann distribution on the reaction center). In models with spectral heterogeneity, $p_{rc}(B) > 1/N$ when all antenna pigments have a peak absorptions at higher energy than that of the reaction center. The models presented by Seely (1973), Shipman (1980), Fetisova et al. (1985), Jean et al. (1989), Pullerits and Freiberg (1991), and Jia et al. (1992), and the PS I and PS II models described above are examples of models with such spectral heterogeneity, whereas the canonical models in Knox (1968) and Pearlstein (1982, 1984, 1992) are not. Note that **p**(B) and $p_i(B)$ are not affected by spatial arrangement or distribution; therefore, funnel and random models with the identical spectral composition will have identical **p**(B).

The Boltzmann distribution is temperature-dependent due to the effect of temperature on absorption and emission lineshapes. With decreasing temperature, rate constants for both forward and reverse transfer will decrease due to smaller overlap of donor and acceptor states. This decrease will be most pronounced for reverse transfer because the 0,1 and 1,0 vibrational bands contribute almost nothing to the overlap integral. In contrast, forward transfer may depend largely on overlap of the vibrational bands at decreased temperature.

The term Boltzmann distribution (or thermal equilibrium) has been previously used to describe the decay of a system when the shape of the time-dependent emission spectra no longer changes with increasing time (van Grondelle, 1985; Feick et al., 1980; Rijgersberg et al., 1980; Schatz et al., 1988; Holzwarth, 1991; Sundström et al., 1986; Borisov, 1990; Owens et al., 1987, 1988, 1989; McCauley et al., 1989; Shipman, 1980). In our terminology, this state is referred to as a transfer equilibrium (TE) state. Boltzmann equilibrium is reserved for the distribution reached at long times in models without decay. In subsequent sections, we will show that **p**(TE) can vary substantially from **p**(B) due to the nature of the dynamics of the system. Some insight into the difference between the Boltzmann (or thermal) and transfer equilibrium distributions have been alluded to by Zankel and Clayton (1969), Rijgersberg et al. (1980), Pearlstein (1982), and Knox (1968).

TRANSFER EQUILIBRIUM PHENOMENON

Equation 2 demonstrates that the decay of the system, $P(t) = \Sigma p_i(t)$, is determined by the eigenvalues (λ_j) and the pre-exponential weighting factors ($c_j x_{ij}$). In the limit as $t \rightarrow \infty$, the contribution to $\mathbf{P}(t)$ from all eigenvalues except one (the smallest or dominant eigenvalue λ_1) will have vanished. Defining t_e as the time at which λ_1 dominates $\mathbf{P}(t)$, it can be shown from Equation 2 that at $t > t_e$, the fraction of the excited state on any pigment (i) when normalized to the total excited state remaining on the model, $\not{p}_i(TE)$, will remain constant

$$\not{p}_i(TE) = \frac{p_i(t > t_c)}{\sum_{m=1}^{N} p_m(t > t_c)} = \frac{x_{i1}}{\sum_{m=1}^{N} x_{m1}} \quad (4)$$

where x_{i1} is the ith element in the eigenvector of λ_1. For convenience, t_e is defined as the time at which $\not{p}_{rc}(t)$ is within 5% of $\not{p}_{rc}(TE)$, where $\not{p}_{rc}(t)$ and $\not{p}_{rc}(TE)$ are the normalized amount of excited state on the reaction center at time t and at TE, respectively. Equation 4 shows that the normalized eigenvector elements of λ_1 (where the sum of eigenvector elements is the normalization factor) are equivalent to the site-dependent fractions of the total excited state remaining on the array at $t > t_e$. We have described this state of $\mathbf{P}(t)$ as the TE state. The TE state is not a true equilibrium in that irreversible loss of the excited state continues (via photochemistry, fluorescence, etc.). However, the rate of loss on each site is such that the normalized distribution remains constant. This situation is equivalent to the zero-mode dominance predicted from analytical solutions to excited state dynamics found by Pearlstein (1982, 1984, 1992), Knox (1968), and Schatz et al. (1988) and to the quasi-steady-state description of Borisov (1990).

EVIDENCE FOR THE OCCURRENCE OF TRANSFER EQUILIBRIUM IN CHLOROPHYLL ANTENNAE

There exists compelling experimental evidence for the occurrence of TE states in the chl antennae of photosynthetic systems. Sundström et al. (1986) discussed the equilibration of exciton density in the spectrally distinct pigment pools in two bacterial antenna systems during the lifetime of the excited state. Owens et al. (1987, 1988, 1989) concluded from several different types of experiments that excited states equilibrate or delocalize among the PS I core chl *a* spectral forms on time scales which were short compared with the photochemically limited lifetime. Holzwarth and coworkers (Turconi et al., 1993; Holzwarth, 1987; Lee et al., 1989) reported complex decay-associated spectra ($\tau < 20$ ps) in both PS I and PS II of green algae and higher plants. These components were also attributed to equilibration of the excited state among the antenna spectral forms on times which are short compared to the excited state lifetimes. McCauley et al. (1989) and Owens et al. (1989) described blue-shifted fluorescence emission when the long wavelength edge of antenna absorption was excited. Similarly, Owens et al. (1988) and Trissl et al. (1993) observed that photochemically limited lifetimes in PS I were independent of excitation on the blue or red edge of the antenna absorption, indicative of delocalization of the excited state among antenna spectral forms. Finally, Schatz et al. (1988), proposed a model for excitation motion and trapping in PS II based upon experimental data (Schatz et al., 1987) which includes rapid equilibration of the excitation among antenna spectral forms and

the reaction center on time scales comparable or shorter than the time resolution of a single-photon-counting fluorescence apparatus. Together, these data strongly indicate that TE states are rapidly established among the chl antennae of PS I and PS II.

Simulations of excitation dynamics in model photosynthetic antennae have also demonstrated the characteristics of TE states. Shipman (1980) stressed the importance of detrapping in order to create a near-thermal equilibrium between the antenna and the reaction center. Jean et al. (1989) showed that the time-dependent evolution of the total emission from PS I-like models changed only during the first 10 ps and remained constant thereafter. Beauregard et al. (1991), using similar simulation protocols, reported that equilibration of the excited state between various spectral forms in spectrally heterogeneous antenna occurs on relatively short time scales. In both studies, equilibration was dependent on rapid (≈1 ps) transfer between antenna sites and is supported by theoretical studies (Owens et al., 1987; Schatz et al., 1988) and by the close packing of chl pigments in vivo (Owens et al., 1989; Kühlbrandt and Wang, 1991; Krauss et al., 1993). The early occurrence of TE states in the excited state decay is completely consistent with the trap-limited description of excited state dynamics in both PS I and PS II (Holzwarth, 1991; Turconi et al., 1993). In bacterial models, Borisov (1990) also suggested that the observation of a TE-like state was a criterion for assigning trap-limited kinetics.

TRANSFER EQUILIBRIUM STATES IN MODELS OF PS I AND PS II

An important consideration of the occurrence of TE states in photosynthetic antennae is the extent to which the TE state contributes to the total decay of the excited state. The experimental data quoted above for PS I and PS II chl pigments suggests that $t_e \leq 0.3\tau$, where τ is the lifetime of the excited states limited by photochemical quenching. Figs. 1 and 2 show $P(t)$ and $p_i(t)$ for representative spectral forms in the PS I and PS II models, where the $p_i(t)$ values represent the normalized fraction of excited state from a single pigment representing that spectral form averaged over the random configurations. Excitation wavelength was 670 and 650 nm for PS I and PS II, respectively. The photochemically limited lifetimes for the models are 73 and 132 ps for the PS I and PS II models, respectively. Both decays are dominated by a single component with an amplitude > 0.95. The results predict experimentally realistic lifetimes (Owens et al., 1987; Holzwarth, 1986). Photochemical yields for the PS I and PS II models are 93 and 87%, respectively.

The occurrence of TE states in our simulations has been monitored directly by plotting $p_i(t)$ for representative spectral forms (Figs. 1 and 2). The data reveal that the TE state is rapidly established (t_e = 24 and 26 ps for PS I and PS II, respectively) in both models even when the initial distribution of excitation is primarily on the highest energy pigments. These values of t_e are consistent with equilibration times

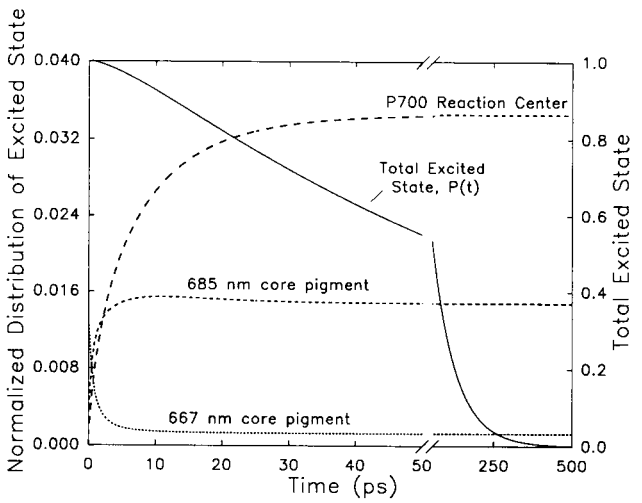

FIGURE 1 Excited state decay (*solid line*; *right ordinate scale*) and time-resolved excited state distributions (*dashed lines*; *left ordinate scale*) for the PS I model with 670-nm excitation. The excited state distributions are presented as that for an individual pigment (as apposed to the sum for the respective spectral form) and have been normalized to the total amount of excited state remaining at any given time. Thus, the excited state distributions are a plot of $p_i(t)$ for selected spectral forms.

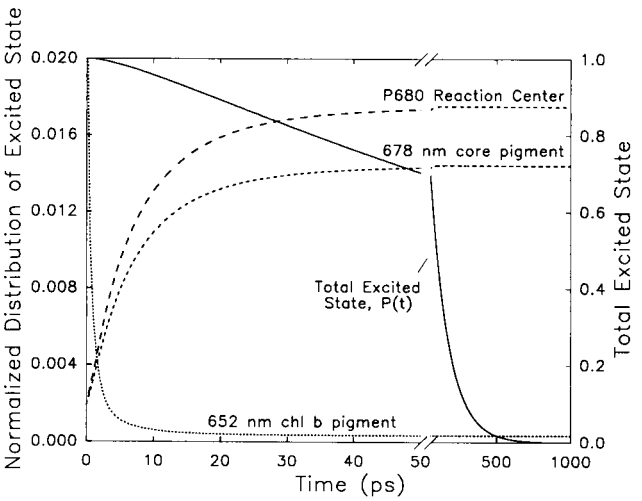

FIGURE 2 Excited state decay (*solid line*; *right ordinate scale*) and time-resolved excited state distributions (*dashed lines*; *left ordinate scale*) for the PS II model with 650 nm excitation. The excited state distributions are presented as that for an individual pigment (as apposed to the sum for the respective spectral form) and have been normalized to the total amount of excited state remaining at any given time. Thus, the excited state distributions are a plot of $p_i(t)$ for selected spectral forms. Note the change in both the *x*- and *y*-axes between Figs. 1 and 2.

determined experimentally (Holzwarth, 1991; Owens et al., 1988). Thus, our PS I and PS II models predict that TE states are established in both photosystems on time scales which are short compared to the photochemically limited lifetime of the excited state. In agreement with previous simulations (Jean et al., 1989; Beauregard et al., 1991), altering either the spatial arrangement, the number of spectral forms, or $\mathbf{p}(0)$ in these models did not alter the qualitative relationship between t_e and τ in either model (data not shown). The only

critical factor is that energy transfer between adjacent pigment sites is rapid, on a time scale of a few picoseconds or less (Jean et al., 1989).

Log plots of P(t) for the same two models (Fig. 3) reveal that in both cases the decay is single exponential except at times less that about $0.5t_e$. The initial nonexponential decay is a manifestation of the structure-dependent dynamics that occurs during the transition from **p**(0) to the TE state (Turconi et al., 1993). Hereafter, decay resulting from a single exponential will be inferred from horizontal plots of $p_i(t)$, since establishment of the TE state corresponds to P(t) being determined by a single eigenvalue, λ_1 (Eqs. 2 and 4). Figs. 1 and 2 show that all pigments reach TE simultaneously indicating that the occurrence of TE can be monitored via any normalized pigment distribution.

These simulations and the experimental data quoted above strongly suggest the occurrence of TE states among the coupled chl pigments of PS I and PS II, and that the TE state may dominate P(t). The occurrence of a TE state implies that all of the structure-dependent excited state dynamics (that can be probed by varying excitation wavelength) occur on time scales that are short compared to t_e. If t_c is comparable to the lifetime of the excited state, then these structure-dependent dynamics dominate the decay. On the other hand, if $t_e < \tau$, the characteristics of the TE state will dominate the total decay. Under these circumstances, decay components associated with the transition from any arbitrary **p**(0) to the TE state (those that may be most revealing in terms of antenna structure), probably occur on time scales which are at or below the limits of detection using single photon counting techniques (Beauregard et al., 1991; Turconi et al., 1993).

Figs. 4 and 5 show a comparison of the TE and Boltzmann distributions for the spectral forms contained in the PS I and PS II models. The bars report normalized distributions on a per pigment basis, while the numbers above the bars indicate the total normalized distribution residing on the spectral form at TE. Due to the large photochemical losses that occur on the reaction center, the TE distribution on the reaction center is less than the corresponding Boltzmann distribution. As a result, TE distributions on antenna pigments are generally greater than their Boltzmann distributions. However, those antenna pigments that are directly coupled to the reaction center (regardless of their energies) exhibit a TE distribution which is lower than that predicted at Boltzmann equilibrium because of the influence of photochemical losses on the reaction center (Fig. 4). Deviations from Boltzmann equilibrium at TE are more dramatic in the PS I model due to the depth of the trap and the inclusion of low energy pigments close to the reaction center (see below). The equilibrium is such that the excited state is almost entirely distributed on chl *a* with only a small fraction (< 2%) found on chl *b* in the PS II model (Fig. 5).

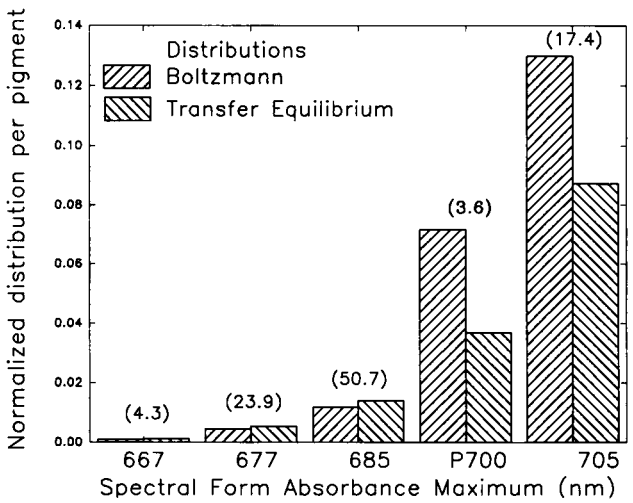

FIGURE 4 Comparison of the Boltzmann distribution and the transfer equilibrium distribution calculated from real chl lineshapes for the core antenna/reaction center complex of PS I. The real chl lineshapes used were that of Shipman and Housman (1979). The data are based upon distributions obtained from analysis of the PS I model described in the models section of this text. The bars represent each of the two distributions normalized on a per pigment basis. The values above the bars show the fractional TE distribution summed over the pigments in each spectral form.

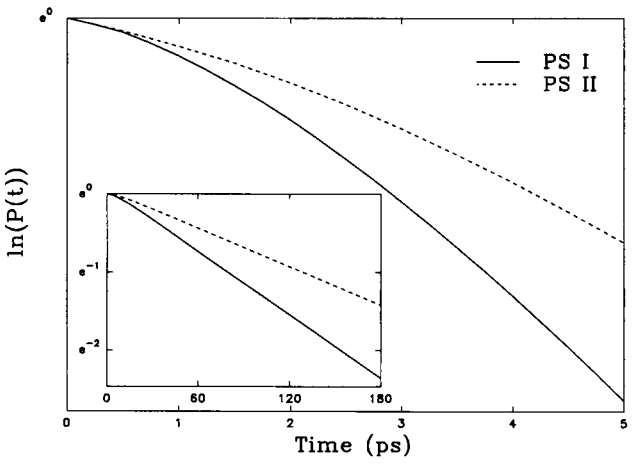

FIGURE 3 Log plot of excited state decays for the PS I and PS II models with 670- and 650-nm excitation, respectively, at both short (main) and long (inset) times.

In the models presented above, photochemistry was treated as an irreversible reaction. Recent experimental (Schatz et al., 1987) and theoretical studies (Schatz et al., 1988; Källebring and Hansson, 1991) and computer simulations (Zipfel, 1993) have shown that reversible electron transport reactions can show up as components of fluorescence decay. In agreement with experiment (Turconi et al., 1993; Schatz et al., 1987), computer simulations have shown that electron transfer influences fluorescence decays in PS II more markedly than in PS I (Zipfel, 1993). Simulation of a system that includes reversible electron transport requires the addition of nonfluorescent sites to the model. Partitioning of excited state between fluorescent and nonfluorescent sites results in a splitting of the photochemically limited lifetime (determined in the absence of electron transfer) into one faster and one or more slower decay components. The faster component represents the removal of excited states from the

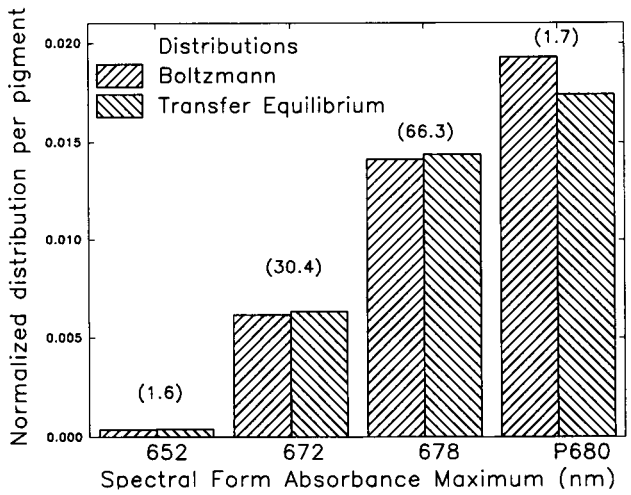

FIGURE 5 Comparison of the Boltzmann distribution and the transfer equilibrium distribution calculated from real chl lineshapes for the PS II complex with two LHC II per core antenna. The real chl lineshapes used were that of Shipman and Housman (1979). The data are based upon distributions obtained from analysis of the PS II model described in the models section of this text with 10-Å spacing between the core and peripheral (LHC II) antennae. The bars represent each of the two distributions normalized on a per pigment basis. The values above the bars show the fractional TE distribution summed over the pigments in each spectral form. Note the change in the *y*-axis between Figs. 4 and 5.

antenna by photochemistry, and the slower component(s) arise from the slow equilibration between the charge transfer states and the antenna via charge recombination. Although addition of electron transport perturbs the TE distribution among the antenna sites (resulting in the faster decay component), it does not significantly alter the rate at which the TE distribution is established or the photochemically limited lifetime (which is, in effect, the weighted average of the faster, antenna-related decay and the slower, electron transport-related component(s)). Therefore, the occurrence and significance of TE states in natural photosynthetic systems can be understood in simpler models that treat k_p as an irreversible step.

MODEL PROPERTIES AFFECTING DECAYS AND TRANSFER EQUILIBRIUM PARAMETERS

Figs. 1 and 2 compare the rate of excited state decay in models of PS I and PS II and show that the decay rate in PS I is approximately twice that of PS II. In any model, the instantaneous rate of excited state decay is given by

$$\frac{d[\Sigma p_i(t)]}{dt} = \frac{d[P(t)]}{dt} = -p_{rc}(t) \cdot k_p - \sum_{i=1}^{N} p_i(t) \cdot k_f \qquad (5)$$

The value of $p_{rc}(t)$ is in general determined by two factors: $\not{\rho}_{rc}(TE)$ at $t > t_e$ and at earlier times by the transition from $\not{\rho}_{rc}(0)$ to $\not{\rho}_{rc}(TE)$. The preceding discussion suggests that in the chl-based antennae of PS I and PS II, the TE state is rapidly established ($t_e < \tau$). In the PS I and PS II models (Figs. 1 and 2), t_e/τ = 24 ps/73 ps = 0.33 and 26 ps/132 ps = 0.20, respectively. When antenna losses are small, substituting for $p_{rc}(t)$ from the left hand equality in Eq. 4, the rate of excited state decay at $t > t_e$ is given by

$$\frac{d[P(t)]}{dt} \approx -P(t) \cdot \not{\rho}_{rc}(TE) \cdot k_p \qquad (6)$$

Thus, in systems where the TE state is rapidly established, $\not{\rho}_{rc}(TE)$ is central to determining the overall rate of decay. The data in Figs. 1 and 2 show that after the first few picoseconds, the value of $\not{\rho}_{rc}(t)$ in the PS I model exceeds that in the PS II model.

In other models, especially those with a wide range of antenna spectral forms (e.g., phycobilisomes), the TE state may be established only very late in the decay (Mullineaux and Holzwarth, 1991), and the transition from **p**(0) to the TE state will dominate the overall decay. In the following sections, we examine the properties of antenna systems which determine both $\not{\rho}_{rc}(TE)$ and the transition from **p**(0) to the TE state.

Properties affecting the normalized fraction of excited state on the reaction center at transfer equilibrium

In models in which the TE state dominates the overall decay ($t_e < \tau$), the simulated lifetime of the excited state is given by

$$\tau = -(\lambda_1)^{-1} = [k_f + k_p \cdot \not{\rho}_{rc}(TE)]^{-1} \qquad (7)$$

where k_f is the sum of all nonphotochemical decay rates in the model. Equation 7 (derived by manipulation of the rate matrix W; Appendix B) explicitly shows the dependence of the excited state lifetime on k_p; however, there is also an implicit dependence on k_p contained in the $\not{\rho}_{rc}(TE)$ parameter. This is because $\not{\rho}_{rc}(TE)$ is determined by the dynamics of excited state motion and k_p has a significant influence on these dynamics. Thus, the dependence of lifetime on k_p is considerably more complex than the simple linear function suggested in Eq. 7.

In a similar manner, excited state motion is also important in determining the fraction of the excited state on the reaction center when $\not{\rho}_{rc}(TE) < p_{rc}(B)$ (Zipfel, 1993). We have defined the parameter %B as a measure of the extent to which the Boltzmann distribution on the reaction center is reached in the TE state

$$\%B = 100 \cdot \left(\frac{\not{\rho}_{rc}(TE)}{p_{rc}(B)}\right) \qquad (8)$$

Equation 8 is a qualitative measure of the influence of dynamics on the TE distribution. In all the models presented, except for ones where there is large spacing either within or between pigment binding volumes, the dynamics retain the general characteristics of a trap-limited model. In models that retain these trap-limited characteristics, %B is usually above 20–30% and has an upper bound of 100%. For models that are relatively more trap-limited, $k_p < k_t$, where k_t is the mean transfer rate constant between nearest-neighbor sites in the

model (Pearlstein, 1982; 1984), we observe that %B and the decay of P(t) are extremely sensitive to the ratio k_p/k_t. In contrast, models that are relatively more diffusion limited exhibit lifetimes and %B values that are largely independent of k_p/k_t (not shown).

Combining Eqs. 7 and 8 gives

$$\tau \simeq -(\lambda_1)^{-1} = \left[k_f + \frac{k_p \cdot p_{rc}(B) \cdot \%B}{100}\right]^{-1} \quad (9)$$

which shows an explicit parameterization of the separate effects of variations in antenna spectral composition, directly affecting $p_{rc}(B)$ and indirectly affecting the dynamics of excited state motion (contained within the %B term), on the photochemically limited lifetime. In addition to the explicit and implicit dependencies of τ on k_p, the lifetime of the excited state also depends on the dynamics of the excited state motion among all of the coupled pigment-binding sites in the model (including the reaction center). In models that reasonably seek to mimic natural photosynthetic systems, analysis of the effects of excited state dynamics on %B must include contributions from transfer between pigment sites within physically separable complexes (e.g., the PS I core complex or LHC I) as well as transfer between these complexes.

The effects of varied coupling between pigments within a defined physical complex were examined using the PS I reaction center/core antenna complex. The coupling between pigments was varied by altering the pigment-binding volume of the complex, and thus the mean spacing between pigment binding sites. The PS I model described above was constructed assuming the complex is composed of a heterodimer of the *psaA* and *psaB* gene products and a specific molecular volume based upon that of LHC II (3300 Å^3/kDa protein (Kühlbrandt and Wang, 1990)). Three additional PS I models with different mean pigment spacings were constructed assuming either a tetrameric aggregation of the *psaA* and *psaB* gene products (Lundell et al., 1985; Owens et al., 1989) and/or using a smaller specific molecular volume of 1500 Å^3/kDa (from the bacterial reaction center (Deisenhofer and Michel, 1989)). The tetrameric aggregation was at one time suggested by a *Chlamydomonas reinhardtii* mutant (strain LM3-A4d) which is known to have a reduced core antenna size of 60 chl/reaction center (half that of wild-type) (Owens et al., 1987, 1989; Zipfel and Owens, 1991) and by quantitative analysis of labeled protein bands in PS I isolated from cyanobacterium *Synechococcus* 6301 revealing four *psaA*/*psaB* gene products per F_{AB} complex (Lundell et al., 1985). The physical properties of the four PS I models along with their decay and TE parameters are summarized in Table 3. The results show that the parameters τ and t_e increase, whereas ϕ_p and %B decrease with increasing mean spacing in the models. The models with the three smallest mean spacings all exhibit lifetimes, photochemical yields, and excited state equilibration times which are in agreement with experimental values despite rather large variations in %B. However, the model with the largest spacing has a lifetime which is more than twice that observed in vivo.

In addition to discussing the effects due to the physical constraints placed upon the pigment binding volume, we must consider the possibility that, although binding within the aggregate may be fixed, that binding between antenna aggregates may be variable. The effects of variations in the coupling of pigment sites between distinct pigment-binding complexes was modeled by altering the distance between LHC II trimers and the PS II core complex in the range of 10–30 Å. The results (Table 4) demonstrate that τ and t_e increase, whereas ϕ_p and %B decrease with decreasing coupling between LHC II and the PS II core. However, only the 10-Å model gives a lifetime and excited state equilibration times that are in agreement with experimental data on small PS II-LHC II aggregates (Holzwarth, 1991; Roelofs et al., 1992). For both the PS I and PS II models, agreement between simulation and experimental data in all cases requires a tight coupling (rapid transfer energy) between pigments, both within pigment-binding complexes and between complexes.

Spectral composition is the sole factor determining the Boltzmann distribution, **p**(B). Spatial arrangement of spectral forms does not affect **p**(B), but it does affect the dynamics of the system (and thus the lifetime and efficiency) via the rate of approach to the TE state and the difference between $p_{rc}(B)$ and $p_{rc}(TE)$ (%B; Eq. 8). Because of the dependence of %B on excited state dynamics, the Boltzmann distribution alone would not be expected to provide useful information on lifetime, efficiency, or valid comparisons between models (Eq. 9). The effects of spectral heterogeneity have been examined in numerous simulation models (Seely, 1973; Shipman, 1980; Fetisova et al., 1985; Jean et al., 1989;

TABLE 3 Excited state lifetimes, photochemical yields, and TE parameters for PS I models with varied coupling between pigments within a defined physical complex

PSI model	Mean spacing	τ	t_e	ϕ_p	%B
	(Å)	(ps)	(ps)		
Small dimer	9.5	42 ± 2	6 ± 1	95.5 ± 0.2	86 ± 3.4
Small tetramer	11.6	60 ± 10	17 ± 4	94.0 ± 0.9	61 ± 9.6
Large dimer	12.6	73 ± 9	24 ± 3	92.6 ± 1.0	49 ± 6.7
Large tetramer	15.8	204 ± 48	52 ± 25	79.2 ± 5.2	16 ± 4.3

Excitation was at 670 nm. The lifetimes presented are that of the photochemically limited decay component $-(\lambda_1)^{-1}$ from the simulation results. The value of t_e is that time at which $p_{rc}(t) = 0.95\,p_{rc}(TE)$. Data is reported as the mean ± S.D. based upon the 15 random configurations. See text for details of the models.

TABLE 4 Excited state lifetimes, photochemical yields, and TE parameters for PS II models with varied coupling between distinct pigment-binding complexes

Spacing between LHC II and the core antenna	τ	t_e	ϕ_p	%B
(Å)	(ps)	(ps)		
10	132 ± 2	26 ± 3	87 ± 0.2	88 ± 2
20	140 ± 3	121 ± 15	84 ± 0.5	80 ± 3
30	220 ± 16	225 ± 43	74 ± 1.5	46 ± 5

Excitation was at 650 nm (i.e., initial excitation was primarily found on the chl *b* pigments contained within LHC II). The lifetime presented is that of the photochemically limited decay component $-(\lambda_1)^{-1}$ from the simulation results. The value of t_e is that time at which $p_{rc}(t) = 0.95 p_{rc}(TE)$. Data is reported as the mean ± S.D. based upon the 15 random configurations. See text for details of the models.

Pullerits and Freiberg, 1991; Jia et al., 1992). The effects of varying spatial arrangement on lifetime (funnel versus random models with a fixed spectral distribution) have also been examined (Fetisova et al., 1985; Jean et al., 1989; Beauregard et al., 1991; Jia et al., 1992). In the first approximation, the primary effects of a funnel-like arrangement compared to a random model would be a directed energy transfer to the reaction center (analogous to a shorter first passage time; Pearlstein, 1984; Beauregard et al., 1991) and an increase in the value of k_{detrap}, where k_{detrap} is defined as the rate constant for transfer from the reaction center (pigment 1 in our notation) to all other antenna sites in the model:

$$k_{detrap} = \sum_{i=2}^{N} F_{i1} \tag{10}$$

In a trap-limited system, both of these effects would be expected to increase %B and thus result in decreased lifetime, equilibration times, and increased photochemical efficiency. However, Jean et al. (1989) and Beauregard et al. (1991) demonstrated that, as the mean spacing between pigments decreased, the difference in excited state lifetime between the funnel and random models vanished. It would appear that the expected effects of a funnel arrangement on %B through shorter first passage time and increased detrapping are balanced at small mean pigment separation by other, nonintuitive effects which make %B relatively insensitive to spatial arrangement of the antenna spectral forms.

The point at which rapid energy transfer between neighboring pigments overcomes the expected differences between random and funnel models is likely to be highly model dependent. However, models incorporating the close spacing (8–15 Å) between nearest neighbor pigments determined from crystallographic data in a variety of bacterial, algal, and plant antenna complexes (Kühlbrandt and Wang, 1991; Krauss et al., 1993; Schirmer et al., 1987; Tronrud et al., 1986) are clearly in the regime where the effect of spatial arrangement on lifetime is negligible (Jean et al., 1989; Beauregard et al., 1991; Zipfel, 1993). However, the pigments immediately adjacent to the reaction center may be an exception to this rule (Jia et al., 1992; Zipfel, 1993).

Properties affecting the transition from the initial to transfer equilibrium distribution

Equally important in understanding the dynamics of excited state motion and the factors that determine excited state lifetime and photochemical efficiency is a description of the processes occurring during the transition from any arbitrary **p**(0) to the TE state. For the PS I and PS I models, it was shown that the TE state is rapidly established in both systems (t_e/τ = 0.27 and 0.10, respectively). In both cases, **p**(0) is such that $p_{rc}(0) < p_{rc}(TE)$, and the decay is complex at early times ($t < 0.5t_e$). In accordance with Eq. 6, the rate of decay increases (Fig. 3) as the value of $p_{rc}(t)$ increases (Figs. 1 and 2). In all cases where $p_{rc}(0) < p_{rc}(TE)$ the decay of $P(t)$ at $t < t_e$ is slower than the decay once the TE state is established. However, in cases where the TE state dominates the decay of $P(t)$, we have found no general relationship between the rate of approach to TE (as measured by t_e or t_e/τ) and the photochemically limited lifetime.

Fig. 6 shows $p_{rc}(t)$ and the decay of excited state (inset) for the PS II model with several **p**(0) distributions determined for excitation wavelengths ranging from 650–690 nm. Important features of this figure are the observations that the TE distributions obtained from different **p**(0) distributions are identical, and that the TE state is rapidly approached regardless of the **p**(0) distribution. During the approach to TE, the value of $p_{rc}(t)$ (and $p_{rc}(t)$) is determined by **p**(0) and the dynamics of the system. For example, with 690-nm excitation, the initial distribution is such that $p_{rc}(0) > p_{rc}(TE)$. However, the kinetics of the transition from **p**(0) to the TE state are nearly identical for any arbitrary

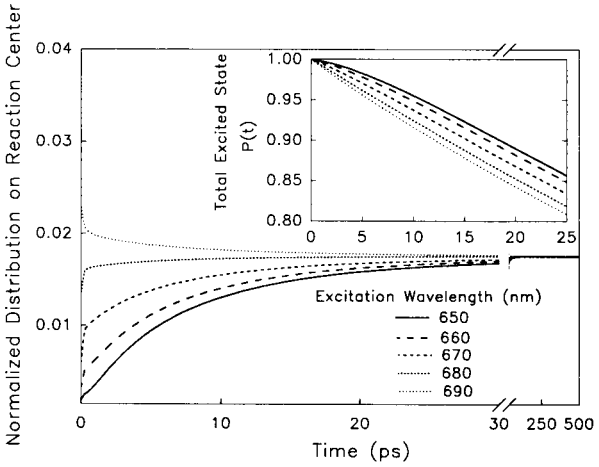

FIGURE 6 Effect of varied excitation wavelength on the approach to TE in well-coupled PS II model. Spacing between the core and peripheral (LHC II) antennae is 10 Å. The approach to TE is monitored as a plot of $p_{rc}(t)$ with varied initial distribution of excited state **p**(0). Excited state decays **P**(t) are also shown (*inset*). The initial distribution of excited state is determined by the relative absorption cross-section of each individual pigment at the excitation wavelength ranging from 650 to 690 nm. Note that the final TE distribution obtained from varied initial excited state distributions is identical (see times greater than 50 ps) and that the TE state is rapidly approached regardless of the initial excited state distribution.

$\mathbf{p}(0)$ (Fig. 6). The most common case for experimental conditions is one in which $p_{rc}(0) < \rho_{rc}(TE)$. Here, the initial dynamics are involved in increasing $\rho_{rc}(t)$ with time. The time where $\rho_{rc}(t) < \rho_{rc}(TE)$ contributes to slower decay of $P(t)$ and decreased ϕ_p. An alternative situation is one where $p_{rc}(0) > \rho_{rc}(TE)$. Here, the limiting case is $p_{rc}(0) = 1$, and this gives the fastest decay possible for the model (as unrealistic as this $\mathbf{p}(0)$ may be). Now the initial dynamics are involved in decreasing $\rho_{rc}(t)$ with time. Time where $\rho_{rc}(t) > \rho_{rc}(TE)$ contributes to faster decay of the system (increased efficiency). This case also demonstrates the problem of determining k_p directly in a trap-limited model. Even if the reaction center can be preferentially excited, a considerable amount of the initial decay of $p_{rc}(t)$ is due to back-transfer to the antenna.

Finally, we consider the special case where $p_{rc}(0) = \rho_{rc}(TE)$, or more specifically $\mathbf{p}(0) = \mathbf{p}(TE)$. Here, dynamics have no direct influence on the decay of $P(t)$, and a single exponential is observed, even with infinite time resolution. In our simulations, a pure single exponential decay can be detected as a solution to the Pauli master equation having a dominant decay component with amplitude of 1.0. In the simulations, $\mathbf{p}(0) = \mathbf{p}(TE)$ is determined from the normalized eigenvector of the dominant eigenvalue (λ_1) as described in Eq. 4. However, obtaining $\mathbf{p}(0) = \mathbf{p}(TE)$ is probably not possible experimentally, although $\mathbf{p}(0) \simeq \mathbf{p}(TE)$ may be. In order to detect such a state, one would need very high time resolution (a few hundred femtoseconds). Note that this analysis includes exponential decay components arising only from antenna structure and not those arising from antenna size heterogeneity or coupling to electron transfer reactions. In the absence of such complications, appropriate variations in $\mathbf{p}(0)$ may be very useful in obtaining structural information from a system even though the TE state may dominate the overall decay. Zipfel (1993) has suggested that knowledge of $\mathbf{p}(TE)$ may impose structural constraints on physical models intended to represent in vivo systems.

In agreement with numerous theoretical and experimental studies (e.g., Jean et al., 1989; Beauregard et al., 1991; Owens et al., 1987; 1988, 1989; Holzwarth et al., 1987), our simulations show that the decay of a sample can vary significantly with changes in excitation wavelength although, depending on the value of t_e, these variations may occur on a time scale that is experimentally inaccessible using the single photon counting technique. According to Eq. 2, the variations in the decay of $P(t)$ with excitation wavelength can only arise because of changes in c_j terms, the constants which scale the eigenvector elements x_{ij} terms to the initial distribution $\mathbf{p}(0)$. Experimentally, this must result in changes in amplitudes and not in lifetimes of decay components. Any apparent changes in lifetime must be attributed to excitation wavelength-dependent changes in the amplitudes of two or more unresolved eigenvalues. The frequent observation of several subdominant eigenvalues of approximately the same magnitude ($0.05\ \lambda_1 < \lambda_i < 0.2\ \lambda_1$) in our simulations suggests that interpretation of decay- or species-associated spectra associated with these lifetimes is difficult at best. The same conclusion has been reached in analysis of experimental systems (Zipfel, 1993; Turconi et al., 1993).

In some models, especially those with a wide range of spectral forms (phycobilisomes are a possible example), TE may be established only very late in the decay and the transition from $\mathbf{p}(0)$ to TE dominates the decay. Simple, smooth transitions from $\mathbf{p}(0)$ to the TE state are typically observed (Figs. 1, 2, and 6); however, eigenvalues other than λ_1 (subdominant eigenvalues), may dominate the decay at $t < t_e$. By extrapolation from our description of TE states, periods of the decay dominated by subdominant eigenvalues may significantly influence the dynamics, lifetime, and photochemical efficiency of a system as shown experimentally in a phycobilisome containing system (Sauer et al. 1988; Holzwarth et al., 1987). The fact that the subdominant eigenvalues are controlling redistribution of excited state from the initial to the TE state on experimentally accessible timescales, indicates that selection of excitation wavelength may determine the degree to which multiexponential decays are observed in large, spectrally diverse systems.

EXPRESSIONS FOR TRANSFER EQUILIBRIUM PARAMETERS

In the above discussion, parameters such as $\rho_{rc}(TE)$ have been emphasized as being important to our understanding of TE and excited state decays. One may ask whether or not these parameters are simple functions of basic model properties. Appendix B contains derivations for two separate and general expressions for the eigenvalues of the rate matrix. Eq. 7 presents the relationship between τ, λ_1, and $\rho_{rc}(TE)$ that is specific for a system in which a TE state dominates the overall decay. The derivation of an alternate expression for the eigenvalues of the rate matrix relating their values to other model parameters is contained within Appendix B and is presented here as an expression for the dominant eigenvalue:

$$\lambda_1 = -k_p - k_f - k_{detrap} + \sum_{i=2}^{N} \left(F_{i1} \cdot \frac{p_1(B)}{p_i(B)} \cdot \frac{x_{i1}}{x_{11}} \right) \qquad (11)$$

Note that the reaction center is denoted as pigment 1 in our notation. Equation 11 suggests relationships between the eigenvalues of the rate matrix and k_p, k_f, k_{detrap}, and a summed expression involving detrapping rate constants, Boltzmann equilibrium levels, and eigenvector elements. The complex term closely resembles k_{detrap} (Eq. 10) but differs in the fact that each detrapping rate constant (F_{i1}) is weighted by terms containing eigenvector elements and Boltzmann distributions before summation.

Equating Eqs. 7 and 11 leads to a useful expression for $\phi_{rc}(TE)$:

$$\phi_{rc}(TE) = 1 + \frac{k_{detrap}}{k_p}\left[1 - \frac{\sum_{i=2}^{N}\left(F_{i1}\cdot\frac{p_1(B)}{p_i(B)}\cdot\frac{x_{i1}}{x_{11}}\right)}{k_{detrap}}\right] \quad (12)$$

Equation 12 shows the importance of the contribution of k_p/k_{detrap} to $\phi_{rc}(TE)$. The k_p/k_{detrap} ratio has previously been suggested to be an important model parameter (Pearlstein, 1982, 1984; Owens et al., 1987) and a similar ratio of k_p/k_t (where k_t is the average rate constant for nearest neighbor transfer) has frequently been the means by which diffusion- and trap-limited models have been differentiated (Pearlstein, 1982, 1984; van Grondelle, 1985). The importance of such a ratio has also been exploited in simulations involving a "focusing zone" around the reaction center, achieved either through structure of the arrays near the reaction center (pigment placement and mutual orientations (Fetisova et al., 1985)) or through spectral heterogeneity via placement of long wavelength pigments near the reaction center (Seely, 1973; Fetisova et al., 1985). The main reason for including these expressions is to demonstrate their complex nature and to stress the fact that excited state dynamics influences all of the important TE parameters except $p_{rc}(B)$ (which depends solely on site energies). The emphasis is that excited state dynamics determines $\phi_{rc}(TE)$ (and %B) in a nonintuitive way; the expression for $\phi_{rc}(TE)$ (Eq. 12) is one which cannot be simply evaluated without knowledge of the complete numerical solution of the Pauli master equation.

COMPARISON WITH OTHER WORK

Pearlstein (1982, 1984, 1992) and Borisov (1990) have presented analytical solutions to excited state dynamics on models of core antenna/reaction center complexes. Of key interest is the comparison of the analytic expressions for the lowest moment of $P(t)$ to that predicted from numerical solutions to the Pauli master equation. In these studies, models of reaction center/core antenna complexes were severely constrained in order to insure a systematic solution to the Pauli master equation. For example, Pearlstein's solutions (1982, 1984, 1992) require equal Förster rate constants between nearest-neighbor sites (therefore, 2D models with isoenergetic antenna pigments placed at lattice sites within a regular array). For simplicity of comparison, we will examine the special case where the reaction center has the same energy as the antenna (Pearlstein, 1982).

The lowest moment of $P(t)$ or M_o is, in general, largely determined by the longest-lived lifetime component. For any situation, M_o is formally the summed or "1/e" lifetime which can be found by integrating $P(t)$ from 0 to ∞. In the context of our simulations,

$$M_o = -\left[\sum_{j=1}^{N}\frac{c_j\sum_{i=1}^{N}x_{ij}}{\lambda_j}\right] \quad (13)$$

Pearlstein's analytic solutions (1982) show that

$$M_o \simeq \alpha\frac{N}{k_t} + \frac{N}{k_p} \quad (14)$$

for both diffusion- and trap-limited systems with uniform ($p_i(0) = 1/N$) initial distributions; α is a parameter based upon the geometry of the 2D lattice. The two terms in Eq. 14 have been assigned to the time it takes the excited state to initially visit the reaction center (the so-called "first passage time") and the lifetime of the excited state after its initial reaction center visit.

Likewise, Borisov (1990) presents a specific analytical solution to excited state dynamics on models of bacterial antenna systems. The nature of the solutions (Eq. 4 in Borisov (1990)) are such that the decay is primarily controlled by a single component given by the following expression:

$$M_o = \left[K_\Sigma + K_c\frac{N_p}{N_p + N}\right]^{-1} \quad (15)$$

The terms K_Σ and K_e are equivalent to our k_f and k_p, and N_p and N are the number of reaction center and antenna pigments, respectively. Equation 15 holds for purely trap-limited systems with intermolecular transfers rate constants between identical antenna molecules tending to ∞. Borisov's solution differs from that of Pearlstein both in the K_Σ term and the lack of influence by the first passage time ($\alpha N/k_t$), whose effect vanishes as $k_t \to \infty$.

In comparison, if we build models using the restrictions required by the analytical solutions above and apply Eq. 7, which requires only that $t_e < \tau$ (an assumption that is probably met for PS I and PS II (Holzwarth, 1991) and bacterial systems), we obtain a different expression for M_o

$$M_o \simeq -(\lambda_1)^{-1} \simeq \left[\frac{1}{k_p\cdot\phi_{rc}(TE)}\right] = \left[\frac{100\cdot N}{k_p\cdot\%B}\right] \quad (16)$$

Equation 16 follows from Eq. 7 when it is expanded to include the facts that 1) $\phi_{rc}(TE) = p_{rc}(B)\cdot\%B$ and 2) $p_{rc}(B)$ for a model with a homogeneous antenna and isoenergetic reaction center is simply $1/N$. Ignoring the small contribution of k_f, Eq. 16 differs from the solutions reported by Pearlstein and Borisov by the factor of %B in the denominator. Because %B can have values between 0 and 100, the analytical solutions underestimate the actual M_o of the model (Eq. 13) and are only correct when %B 100. However, in models which are trap-limited, the extent to which Boltzmann equilibrium on the reaction center is reached can be as low as 30%, as discussed previously. Therefore, %B may be much less than 100% in PS I, PS II, and bacterial antenna systems which are believed to be trap-limited (Holzwarth, 1991; Owens et al., 1989; Borisov, 1990). The differences between the analytic and numeric solutions must be due to mathematical assumptions used to derive the analytical solutions.

Not only are the analytical solutions accurate only in the case where %B $\approx$ 100, they are also deficient in addressing

naturally occurring spectral heterogeneity and geometric factors such as spatial arrangement and mutual orientation which can dramatically influence decays through their affects on the dynamics of the system. Also, the assumption of homogeneous antennae (with or without isoenergetic reaction centers) can lead to large errors when estimating the Boltzmann distribution on the reaction center. Since both bacterial and higher plant antennae are known to be spectrally heterogeneous with pigments both of higher and lower energy than that of the reaction center, $p_{rc}(B)$ may be quite different than $1/N$. Thus, the applicability of such analytical solutions is severely restricted to specific models which may bear little resemblance to in vivo systems. Finally, comparison of the analytical and numerical solutions redirects the emphasis of excited state dynamics from experimentally inaccessible parameters such as "first passage time" and the lifetime of the excited state after its initial visit to the reaction center to an understanding of the importance of the normalized fraction of excited state on the reaction center at TE, $\rho_{rc}(TE)$ (Eqs. 7 and 17).

SUMMARY

In these simulations, we have attempted to use realistic structural and spectral information and appropriate physical laws to calculate the time-dependent properties of excited state decay in the chl-based antennae of PS I and PS II. Where detailed spectral or structural data is lacking, we have assumed that we know the correct in vivo spectra and applied the appropriate overlap calculations and averaged over random spatial configurations. Similarly, we have assumed that energy transfer occurs only by dipole interactions. Altering these assumptions would quantitatively change the data presented, but it would not modify the conclusion that transfer equilibrium states are a requisite component of any system which models antenna processes and primary photochemistry as a system of coupled, first-order differential equations. The only requirement is that the system is tightly coupled: energy transfer between neighboring sites be on the time scale of a few picoseconds or less (Jean et al., 1989; Beauregard et al., 1991).

Although the concept of transfer equilibrium is rather simple, the consequences of its occurrence are significant. After a certain time (t_e), which is model- and $\mathbf{p}(0)$-dependent, the contribution to the model's total decay from all eigenvalues except one (λ_1) will have vanished and the fractional distribution of the excited state among coupled pigments remains constant over time. The transfer equilibrium which we describe differs from Boltzmann equilibrium (the state of a model without decay at infinite time) due to the nature of excited state migration and trapping. The contribution of the TE state to the total decay depends on when the TE state is established in the decay of $P(t)$. If TE is established rapidly compared to the lifetime of the excited state ($t_e < \tau$), then the properties of the TE state dominate the decay. In agreement with previous experimental studies (Turconi et al., 1993; Roelofs et al., 1992; Owens et al., 1987, 1989), we provide evidence that TE states are rapidly established in the chl-based antennae of both PS I and PS II on time scales that are short compared to their photochemically limited lifetimes. Properties of the TE state dominate key observables. In particular, the normalized fraction on the reaction center at TE is directly proportional to the excited state lifetime. Thus, knowledge of the excited state distribution of the TE state is central to determining the overall excited state lifetime and photochemical efficiency of the system. Finally, the results from the models of PS I and PS II demonstrate the power of simulations and TE parameters in selecting between various physical models to describe experimental results.

We thank J. W. Lee, C. Ting, A. Ganago, I. Ganago, and R. Knox for helpful discussions and insightful comments.

This research was supported by grants (to T. G. O.) from the National Science Foundation (DMB 8803626 and DMB 9005574). P. D. L. was supported by an A. D. White fellowship from Cornell University. W. Z. and P. D. L. acknowledge support from a National Institutes of Health training grant in Molecular Physics of Biological Systems (08-T26 M08267A).

APPENDIX A

Definition of TE terms found throughout the text and appendices

N	number of pigment binding sites in model
E_i	peak absorption (energy) of pigment i
F_{ij}	Förster rate constant for transfer from pigment j to i
k_p	photochemical rate constant
k_f	summation of all nonphotochemical unimolecular decay rates
k_t	mean transfer rate constant between nearest-neighbor pigments in the model
$\mathbf{W}$	$N \times N$ rate matrix of pairwise transfer rates and unimolecular decay rates
λ_j	jth eigenvalue of $\mathbf{W}$
λ_1	smallest or dominant eigenvalue of $\mathbf{W}$
x_j	$N \times 1$ eigenvector of $\mathbf{W}$ corresponding to λ_j with eigenvector elements x_{ij}
x_{ij}	individual eigenvector elements; subscript i refers to pigment, j to eigenvalue
c_j	arbitrary constants in general solution chosen such that $\mathbf{p}(t)$ at $t = 0$ equals $\mathbf{p}(0)$
TE	transfer equilibrium
t_e	time at which transfer equilibrium is reached; defined as time at which $\rho_{rc}(t) = 0.95_{rc}(TE)$
τ	$1/e$ lifetime of the excited state (photochemically limited)
$p_i(t)$	time-dependent site occupation probability for pigment i at time t
$\mathbf{p}(t)$	vector of site occupation probabilities at time t
$P(t)$	total excited state remaining at time t; $P(t) = \Sigma p_i(t)$
$p_i(0)$	initial distribution of excitation on pigment i
$\mathbf{p}(0)$	vector of initial distribution of excitation
$\rho_i(t)$	normalized time-dependent site occupation probability for pigment i; $_i(t) = (p_i(t)/\Sigma p_i(t))$

ρ_i(TE)	normalized amount of excitation residing on pigment i at transfer equilibrium
p(TE)	vector of transfer equilibrium distribution of excited state
p_i(B)	Boltzmann population on pigment i obtained from simulations of models with no decay
p(B)	Boltzmann distribution at 298 K obtained from simulations of models with no decay
%B	percentage of Boltzmann population reached on the reaction center at transfer equilibrium
J	$N \times N$ square matrix with all elements of unity
pigment 1	reaction center capable of photochemistry (also denoted as "rc" subscript in text)
k_{detrap}	sum of rate constants for transfer of excitation from the reaction center to antenna pigments
$\mathbf{W}\mathbf{x}_j = \lambda_j\mathbf{x}_j$	the eigenvalue equation

Expanded format of the rate matrix W

$$\mathbf{W} = \begin{bmatrix} -(k_p + k_f + \sum F_{i1}) & F_{12} & \cdots & \cdots & \cdots & F_{1N} \\ F_{21} & -(k_f + \sum F_{i2}) & F_{23} & \cdots & \cdots & F_{2N} \\ F_{31} & F_{32} & -(k_f + \sum F_{i3}) & F_{34} & \cdots & F_{3N} \\ \vdots & \vdots & \ddots & & & \vdots \\ \vdots & \vdots & & \ddots & & \vdots \\ \vdots & \vdots & & & \ddots & \vdots \\ F_{N1} & \cdots & \cdots & \cdots & F_{N,N-1} & (k_f + \sum F_{iN}) \end{bmatrix}$$

APPENDIX B

Derivation of expressions for the eigenvalues of the system

1) Derivation of the expression relating the eigenvalues of the system to the values of k_f, k_p, and the eigenvalue's normalized eigenvector elements. The derivation initiates by multiplying both sides of the eigenvalue equation involving the rate matrix **W** by a special square matrix, the **J** matrix.

$$\mathbf{J}\mathbf{W}\mathbf{x}_j = \mathbf{J}\lambda_j\mathbf{x}_j = \lambda_j\mathbf{J}\mathbf{x}_j \tag{B1}$$

The left-hand side of Eq. B1 is easily simplified to an $N \times 1$ matrix through a series of matrix multiplication steps. In the first step, the rate matrix is multiplied from the left by the **J** matrix resulting in an $N \times N$ matrix:

$$\mathbf{J}\mathbf{W} = \begin{bmatrix} -(k_p + k_f) & -k_f & \cdots & -k_f \\ \vdots & \vdots & \ddots & \vdots \\ -(k_p + k_f) & -k_f & \cdots & -k_f \end{bmatrix} \tag{B2}$$

Next, if the vector $\mathbf{x}_j$ is multiplied from the left by the resulting matrix in Eq. B2 and one notes that

$$-(k_p + k_f)x_{1j} - k_f\sum_{i=2}^{N} x_{ij} = -k_p x_{1j} - k_f\sum_i x_{ij} \tag{B3}$$

then the desired simplification of the left-hand side of Eq. B1 (an $N \times 1$ matrix) is obtained:

$$\mathbf{J}\mathbf{W}\mathbf{x}_j = \begin{bmatrix} -k_p x_{1j} - k_f\sum_i x_{ij} \\ \vdots \\ -k_p x_{1j} - k_f\sum_i x_{ij} \end{bmatrix} \tag{B4}$$

Likewise, the right-hand side of Eq. B1 is easily simplified to an $N \times 1$ matrix through matrix multiplication. First, the eigenvector $\mathbf{x}_j$ is multiplied from the left by the **J** matrix followed by scalar multiplicaion of the resultant matrix by λ_j to obtain the desired outcome found in Eq. B5.

$$\lambda_j\mathbf{J}\mathbf{x}_j = \lambda_j\begin{bmatrix} \sum_i x_{ij} \\ \vdots \\ \sum_i x_{ij} \end{bmatrix} = \begin{bmatrix} \lambda_j\sum_i x_{ij} \\ \vdots \\ \lambda_j\sum_i x_{ij} \end{bmatrix} \tag{B5}$$

If the top row of the matrix found in Eq. B4 is equated with the top rows of the matrix found in Eq. B5, then the following expression is obtained:

$$-k_p x_{1j} - k_f\sum_i x_{ij} = \lambda_j\sum_i x_{ij} \tag{B6}$$

Dividing both sides of Eq. B6 by Σx_{ij} results in a general expression for the eigenvalues of **W** as a function of k_f, k_p, and its respective eigenvector elements.

$$\lambda_j = -\left[k_f + k_p \cdot \frac{x_{1j}}{\sum x_{ij}}\right] \tag{B7}$$

Equation B7 is completely general and holds for any system independent of the contribution of the TE state to the total decay. In models where the TE state is quickly established and dominates the decay, the resulting τ is predicted by $(\lambda_1)^{-1}$. Replacing $x_{1j}/\Sigma x_{ij}$ with ρ_{rc}(TE) from Eq. 4 in the text as the reaction center is denoted as pigment 1 in our Förster rate constant and eigenvector notation, one obtains:

$$\tau \approx -(\lambda_1)^{-1} = [k_f + k_p(\rho_{rc}(\text{TE}))]^{-1} \tag{B8}$$

2) Derivation of the expression relating the eigenvalues of the system to the values of k_p, k_{detrap}, and %B. As in the first derivation of Appendix B, the derivation initiates with the eigenvalue equation.

Simplification of the left-hand side of the eigenvalue equation via matrix multiplication leads to the $N \times 1$ matrix found in Eq. B9. The subscript m

is temporarily introduced in the summation notation to represent simultaneously the pigment in the eigenvector elements and the donor pigment in the Förster rate constants.

$$\mathbf{W}x_j = \begin{bmatrix} -\left(k_p + k_f + \sum_{i=2}^{N} F_{i1}\right)x_{1j} + \sum_{m=2}^{N} F_{1m}x_{mj} \\ F_{21}x_{1j} - \left(k_f + F_{12} + \sum_{i=3}^{N} F_{i2}\right)x_{2j} + \sum_{m=3}^{N} F_{2m}x_{mj} \\ \vdots \\ \sum_{m=1}^{N-2} F_{N-1,m}x_{mj} - \left(k_f + \sum_{i=1}^{N-2} F_{i,N-1} + F_{N,N-1}\right)x_{N-1,j} + F_{N-1,N}x_{Nj} \\ \sum_{m=1}^{N-1} F_{Nm}x_{mj} - \left(k_f + \sum_{i=1}^{N-1} F_{iN}\right)x_{Nj} \end{bmatrix} \tag{B9}$$

Simplification of the right-hand side of the eigenvalue equation via matrix multiplication leads also to an $N \times 1$ matrix

$$\lambda_j \mathbf{x}_j = \begin{bmatrix} \lambda_j x_{1j} \\ \vdots \\ \lambda_j x_{Nj} \end{bmatrix} \tag{B10}$$

If the rows of the matrix found in Eq. B9 are equated with the rows of the matrix found in Eq. B10, then N expressions are obtained—the first of which is presented in Eq. B11.

$$-\left(k_p + k_f + \sum_{i=2}^{N} F_{i1}\right)x_{1j} + \sum_{m=2}^{N} F_{1m}x_{mj} = \lambda_j x_{1j} \tag{B11}$$

Dividing both sides of Eq. B11 by the first eigenvector element x_{1j}, the following expression results:

$$-\left(k_p + k_f + \sum_{i=2}^{N} F_{i1}\right) + \sum_{m=2}^{N}\left[F_{1m} \cdot \frac{x_{mj}}{x_{1j}}\right] = \lambda_j \tag{B12}$$

In models with no decay at infinite time, an expression equating the rate of excitation transfer from pigment i to pigment j with the rate of excitation transfer from pigment j to pigment i may be proposed.

$$F_{ji} \cdot p_i(B) = F_{ij} \cdot p_j(B) \tag{B13}$$

Rearrangement of Eq. B13 leads to the following expression:

$$F_{ij} = F_{ji} \cdot \frac{p_i(B)}{p_j(B)} \tag{B14}$$

Replacing F_{1m} in Eq. B12 with its equivalent from Eq. B14 (which eliminates the need for the m subscript) yields:

$$-\left(k_p + k_f + \sum_{i=2}^{N} F_{i1}\right) + \sum_{i=2}^{N}\left[F_{i1} \cdot \frac{p_1(B)}{p_i(B)} \cdot \frac{x_{ij}}{x_{1j}}\right] = \lambda_j \tag{B15}$$

Using the definition of k_{detrap} from Eq. 10 in the text, then B15 can be expressed equivalently as

$$-k_p - k_f - k_{detrap} + \sum_{i=2}^{N}\left[F_{i1} \cdot \frac{p_1(B)}{p_i(B)} \cdot \frac{x_{ij}}{x_{1j}}\right] = \lambda_j \tag{B16}$$

Subsequently, if (*a*) the eigenvector x_j is normalized in such a way that the normalization factor is the sum of its elements and (*b*) one defines the percentage of the Boltzmann population reached at transfer equilibrium (%B) as $x_{1j}/p_{rc}(B)$, then the following expression is an alternate form of Eq. B16.

$$-k_p - k_f - k_{detrap} + \sum_{i=2}^{N}\left[\frac{F_{i1} \cdot x_{ij}}{\%B \cdot p_i(B)}\right] = \lambda_j \tag{B17}$$

REFERENCES

Alt, J., J. Morris, P. Westhoff, and R. G. Herrmann. 1984. Nucleotide sequence of the clustered genes for the 44-kDa chlorophyll *a* apoprotein and the 32-kDa-like' protein of the photosystem II reaction center in the spinach plastid chromosome. *Curr. Genet.* 8:597–606.

Atkins, P. W. 1990. *Physical Chemistry*, 4th ed. W. H. Freeman. New York. 995 pp.

Bassi, R., F. Rigoni, and G. M. Giacometti. 1990. Chlorophyll binding proteins with antenna function in higher plants and green algae. *Photochem. Photobiol.* 52:1187–1206.

Beauregard, M., I. Martin, and A. R. Holzwarth. 1991. Kinetic modelling of exciton migration in photosynthetic systems. (1) Effects of pigment heterogeneity and antenna topography on exciton kinetics and charge separation yields. *Biochim. Biophys. Acta.* 1060:271–283.

Biggins, J., and D. Bruce. 1988. Regulation of excitation energy transfer in organisms containing phycobilins. *Photosyn. Res.* 20:1–34.

Borisov, A. Y. 1990. Energy migration in purple bacteria. The criterion for discrimination between migration- and trapping- limited photosynthetic units. *Photosyn. Res.* 23:283–289.

Bruce, D., J. Biggins, T. Steiner, and M. Thewalt. 1985. Mechanism of the light state transition in photosynthesis. IV. Picosecond fluorescence spectroscopy of *Anacystis nidulans* and *Porphyridium cruentum* in state 1 and state 2 at 77 K. *Biochim. Biophys. Acta.* 806:237–246.

Bruce, D., C. Hanzlik, L. N. Hancock, J. Biggins, and R. S. Knox. 1986. Energy distribution in the photochemical apparatus of *Prophyridium cruentum:* picosecond fluorescence spectroscopy of cells in state 1 and state 2 at 77 K. *Photosyn. Res.* 10:283–290.

Bruce, B. D., and R. Malkin. 1988. Structural aspects of photosystem I from *Dunaliella salina. Plant Physiol.* 88:1201–1206.

Butler, W. L. 1961. A far-red absorbing form of chlorophyll, in vivo. *Arch. Biochem. Biophys.* 93:413–422.

Cantrell, A., and D. A. Bryant. 1987. Molecular cloning and nucleotide sequence of the pea psaA and psaB genes of cyanobacterium *Synechococcus* PCC 7002. *Plant Mol. Biol.* 9:453–468.

Chang, J. C. 1977. Monopole effects on electronic excitation interactions between large molecules. I. Application to energy transfer in chlorophylls. *J. Chem. Phys.* 67:3901–3909.

Deisenhofer, J., and H. Michel. 1989. The photosynthetic reaction centre from the purple bacterium *Rhodopseudomonas viridis. EMBO J.* 8: 2149–2170.

Dekker, J. P., E. J. Boekema, H. T. Witt, and M Rögner. 1988. Refined purification and further characterization of oxygen-evolving and tris-treated photosystem II particles from the thermophilic cyanobacterium *Synechococcus* sp. *Biochim. Biophys. Acta.* 936:307–318.

Feick R., R. van Grondelle, C. P Rijgersberg, and G. Drews. 1980. Fluorescence emission by wild-type- and mutant-strains of *Rhodopseudomonas capsulata. Biochim. Biophys. Acta.* 593:241–253.

Fetisova, Z. G., A. Y. Borisov, and M. V. Fok. 1985. Analysis of structure-function correlations in light-harvesting photosynthetic antenna: structure optimization parameters. *J. Theor. Biol.* 112:41–75.

Fish, L. E., U. Kück, and L. Bogorad. 1985. Two partially homologous adjacent light-inducible maize chloroplast genes encoding polypeptides of the P700 chlorophyll a-protein complex of photosystem I. *J. Biol. Chem.* 260:1413–1421.

Förster, T. 1965. Delocalized excitation and excitation transfer. *In* Modern Quantum Chemistry. Vol III. O. Sinanoglu, editor. Academic Press, Inc., New York. 93–137.

Golbeck, J. H. 1987. Structure, function, and organization of the photosystem I reaction center complex. *Biochim. Biophys. Acta.* 895:167–204.

Golbeck, J. H., and D. A. Bryant. 1991. Photosystem I. *In* Current Topics in Bioenergetics. Vol 16. C. P. Lee, editor. Academic Press, San Diego, CA. 83–177.

Hansson, Ö., and T. Wydrzynski. 1990. Current perceptions of photosystem II. *Photosyn. Res.* 23:131–162.

Heitler, W. 1954. *The quantum theory of radiation*, 3rd ed. Oxford University Press, London. 430 pp.

Holzwarth, A. R. 1986. Fluorescence lifetimes in photosynthetic systems. *Photochem. Photobiol.* 43:707–725.

Holzwarth, A. R. 1987. A model for the functional antenna organization and energy distribution in the photosynthetic apparatus of higher plants and green algae. *In* Progress in Photosynthesis Research. Vol 1. J. Biggins, editor. Martinus Nijhoff, Dordrecht. 53–60.

Holzwarth, A. R. 1989. Applications of ultrafast laser spectroscopy for the

study of biological systems. *Quart. Rev. Biophys.* 22:239–326.

Holzwarth, A. R. 1991. Excited state kinetics in chlorophyll systems and its relationship to the functional organization of the photosystems. *In* The Chlorophylls, H. Scheer, editor. CRC Press, Boca Raton. 1125–1151.

Holzwarth, A. R., J. Wendler, and G. W. Suter. 1987. Studies on chromophore coupling in isolated phycobiliproteins. II. Picosecond energy transfer kinetics and time-resolved fluorescence spectra of C-phycocyanin from *Synechococcus 6301* as a function of the aggregation state. *Biophys. J.* 51:1–12.

Jean, J. M., C. K. Chan, G. R. Fleming, and T. G. Owens. 1989. Excitation transport and trapping on spectrally disordered lattices. *Biophys. J.* 56: 1203–1215.

Jennings, R. C., G. Zucchelli, and F. M. Garhaschi. 1990. Excitation energy transfer from the chlorophyll spectral forms to Photosystem II reaction centres: a fluorescence induction study. *Biochim. Biophys. Acta.* 1016: 259–265.

Jia, Y., J. M. Jean, M. M. Werst, C.-K. Chan, and G. R. Fleming. 1992. Simulations of the temperature dependence of energy transfer in the PS I core antenna. *Biophys. J.* 63:259–273.

Källebring, B., and Ö. Hansson. 1991. A theoretical study of the effect of charge recombination on the transfer and trapping of excitation energy in photosynthesis. *Chem. Phys.* 149:361–372.

Knox, R. S. 1968. On the theory of trapping of excitation in the photosynthetic unit. *J. Theor. Biol.* 21:244–259.

Knox, R. S. 1986. Trapping events in light-harvesting assemblies. Theory and modeling of excitation delocalization and trapping. *In* Encyclopedia of Plant Physiology, New Series. L. A. Staehelin and C. J. Arntzen, editors. Springer-Verlag, New York. 286–298.

Knox, R., and D. Gülen 1993. Theory of polarized fluorescence from molecular pairs: Förster transfer al large electronic coupling. *Photochem. Photobiol.* 57:40–43

Knox, R., and S. Lin. 1988. Time resolution and kinetics of "F680" at low temperatures in spinach chloroplasts. *In* Photosynthetic Light-Harvesting Systems. H. Scheer and S. Schneider, editors. Walter de Gruyter & Co., New York. 567–577.

Krauss, N., W. Hinrichs, I. Witt, P. Fromme, W. Pritzkow, Z. Dauter, C. Betzel, K. S. Wilson, H. T. Witt, and W. Saenger. 1993. Three-dimensional structure of system I of photosynthesis at 6 Å resolution. *Nature (Lond.).* 361:326–331.

Kühlbrandt, W., and D. N. Wang. 1991. Three-dimensional structure of plant light-harvesting complex determined by electron crystallography. *Nature (Lond.).* 350:130–134.

Lee, C. H., T. A. Roelofs, and A. R. Holzwarth. 1990. Target analysis of picosecond fluorescence kinetics in green algae: characterization of pirmary processes in photosystem II alpha and beta. *In* Current Research in Photosynthesis. Vol 1. M. Baltscheffsky, editor. Kluwer Academic Publishers, Dordrecht. 387–390.

Lin, S., and R. S. Knox. 1988. Time resolution of a short-wavelength chloroplast fluorescence component at low temperature. *J. Lumin.* 40 & 41: 209–210.

Lin, S., and R. S. Knox. 1991. Studies of excitation energy transfer within the green alga *Chlamydomonas reinhardtii* and its mutants at 77 K. *Photosyn. Res.* 27:157–168.

Lundell, D. J., A. N. Glazer, A. Melis, and R. Malkin. 1985. Characterization of a cynanobacterial photosystem I complex. *J. Biol. Chem.* 260:646–654.

McCauley, S., E. Bittersmann, and A. R. Holzwarth. 1989. Time-resolved ultrafast blue-shifted fluorescence from pea chloroplasts. *FEBS Lett.* 249: 285–288.

Montroll, E. W. 1969. Random walks on latices. III. Claculation of first passage times with application to exciton trapping on photosynthetic units. *J. Math. Phys.* 10:753–765.

Moog, R. S., A. Kuki, M. D. Fayer, and S. G. Boxer. 1984. Excitation transport and trapping in a synthetic chlorophyllide substituted hemoglobin: orientation of the chlorophyll S_1 transition dipole. *Biochemistry.* 23:1564–1571.

Mullineaux, C. W., and A. R. Holzwarth. 1991. Kinetics of excitation energy transfer in the cyanobacterial phycobilisome-Photosystem II complex. *Biochim. Biophys. Acta.* 1098:68–78.

Nanba, O., and K. Satoh. 1987. Isolation of a photosystem II reaction center consisting of D-1 and D-2 polypeptides and cytochrome *b*-559. *Proc. Natl. Acad. Sci. USA.* 84:109–112.

Owens, T. G., S. P. Webb, R. S. Alberte, L. Mets, and G. R. Fleming. 1988. Antenna structure and excitation dynamics in photosystem I. I. Studies of detergent isolated photosystem I preparations using time-resolved fluorescence analysis. *Biophys. J.* 53:733–745.

Owens, T. G., S. P. Webb, L. Mets, R. S. Alberte, and G. R. Fleming. 1987. Antenna size dependence of fluorescence decay in the core antenna of photosystem I: estimates of charge separation and energy transfer rates. *Proc. Nat. Acad. Sci. USA.* 84:1532–1536.

Owens, T. G., S. P. Webb, L. Mets, R. S. Alberte, and G. R. Fleming. 1989. Antenna structure and excitation dynamics in photosystem I. II. Studies with mutants of *Chlamydomonas rheinhardtii* lacking photosystem II. *Biophys. J.* 56:95–106.

Pearlstein, R. M. 1982. Exciton migration and trapping in photosynthesis. *Photochem. Photobiol.* 35:835–844.

Pearlstein, R. M. 1984. Photosynthetic exciton migration and trapping. *In* Advances in Photosynthesis Research. Vol 1. C. Synbesma, editor. Martinus Nijhoff, The Hague. 1:13–20.

Pearlstein, R. M. 1992. Kinetics of exciton trapping by monocoordinate reaction centers. *J. Lumin.* 51:139–147.

Pullerits, T., and A. Freiberg. 1991. Picosecond fluorescence of simple photosynthetic membranes: evidence of spectral inhomogeneity and directed energy transfer. *Chem. Phys.* 149:409–418.

Rijgersberg, C. P., R. van Grondelle, and J. Amesz. 1980. Energy transfer and bacteriochlorophyll fluorescence in purple bacteria at low temperature. *Biochim. Biophys. Acta.* 592:53–64.

Robinson, G. W. 1967. Excitation transfer and trapping in photosynthesis. *Brookhaven Symp. Biol.* 19:16–48.

Roelofs, T. A., C. H. Lee, and A. R. Holzwarth. 1992. Global target analysis of picosecond chlorophyll fluorescence kinetics from pea chloroplasts: a new approach to the characterization of the primary processes in photosystem II α- and β-units. *Biophys. J.* 61:1147–1163.

Ross, R. T., and M. Calvin. 1967. Thermodynamics of light emission and free-energy storage in photosynthesis. *Biophys. J.* 7:595–614.

Rutherford, A. W., and P. Sétif. 1990. Orientation of P700, the primary electron donor of photosystem I. *Biochim. Biophys. Acta.* 1019:128–132.

Sauer, K., and H. Scheer. 1988. Excitation transfer in C-phycocyanin: Förster transfer rate and exciton calculations based on new crystal structure data for C-phycocyanins from *Agmenellum quadruplicatum* and *Mastigocladus laminosus. Biochim. Biophys. Acta.* 936:157–170.

Schatz, G. H., H. Brock, and A. R. Holzwarth. 1987. Picosecond kinetics of fluorescence and of absorbance changes in photosystem II particles excited at low photon density. *Proc. Natl. Acad. Sci. USA.* 84:8414–8418.

Schatz, G. H., H. Brock, and A. R. Holzwarth. 1988. Kinetics and energetic model for the primary processes in photosystem II. *Biophys. J.* 54: 397–405.

Schirmer, T., W. Bode, and R. Huber. 1987. Refined three-dimensional structures of two cyanobacterial C-phycocyanins at 2:1 and 2.5 Å resolution. *J. Mol. Biol.* 196:677–695.

Seely, G. R. 1973. Effects of spectral variety and molecular orientation on energy trapping in the photosynthetic unit: a model calculation. *J. Theor. Biol.* 40:173–187.

Shipman, L. L. 1980. A theoretical study of excitons in chlorophyll *a* on a picosecond timescale. *Photochem. Photobiol.* 31:157–167.

Shipman, L. L., and D. L. Housman 1979. Förster transfer rates for Chlorophyll *a*. *Photochem. Photobiol.* 29:1163–1167.

Sundström, V., R. van Grondelle, H. Bergström, E. Åkesson, and T. Gillbro. 1986. Excitation-energy transport in the bacteriochlorophyll antenna systems of *Rhodospirillum rubrum* and *Rhodobacter sphaeroides* studied by low-intensity picosecond absorption spectroscopy. *Biochim. Biophys. Acta.* 851:431–446.

Suter, G. W., and A. R. Holzwarth. 1987. A kinetic model for the energy transfer in physobilisomes. *Biophys. J.* 52:673–683.

Teller, D. C. 1976. Accessible area, packing volumes, and interaction surfaces of globular proteins. *Nature (Lond.).* 260:729–731.

Trissl, H. W., B. Hecks, and K. Wulf. 1993. Invariable trapping times in photosystem I upon excitation of minor long-wavelength-absorbing pigments. *Photochem. Photobiol.* 57:108–112.

Tronrud, D. E., M. F. Schmid, and B. W. Matthews. 1986. Structure and

X-ray amino acid sequence of a bacteriochlorophyll *a* protein from *Prosthecochloris aestuarii* refined at 1:9 Å resolution. *J. Mol. Biol.* 188: 443–454.

Turconi, S., G. Schweitzer, and A. R. Holzwarth. 1993. Temperature dependence of picosecond fluorescence kinetics of a cyanobacterial photosystem I particle. *Photochem. Photobiol.* 57:113–119.

van Grondelle, R. 1985. Excitation energy transfer, trapping and annihilation in photosynthetic systems. *Biochim. Biophys. Acta.* 811:147–195.

van Kampen, N. G. 1981. Stochastic Processes in Physics and Chemistry. North-Holland Publishing Company. New York. 419 pp.

Werst, M., Y. Jia, L. Mets, and G. R. Fleming. 1992. Energy transfer and trapping in the photosystem I core antenna. A temperature study. *Biophys. J.* 61:868–878.

Wittmershaus, B., T. M. Nordlund, W. H. Knox, R. S. Knox, N. E. Geacintov, and J. Breton. 1985. Picosecond studies at 77 K of energy trnasfer in chloroplasts at low and high excitation intensities. *Biochim. Biophys. Acta.* 806:93–106.

Zankel, K. L., and R. K. Clayton. 1969. Uphill energy transfer in a photosynthetic bacterium. *Photochem. Photobiol.* 9:7–15.

Zipfel, W. 1993. Modelling photon capture, excitation energy transfer, and charge transfer kinetics in photosynthesis. Ph.D. thesis. Cornell University. 290 pp.

Zipfel, W., and T. G. Owens. 1991. Calculation of absolute photosystem I absorption cross-sections from P700 photo-oxidation kinetics. *Photosyn. Res.* 29:23–35.